

## Chapter 6

### **Backbone Cleavage of an Unstructured Region of the GABA<sub>A</sub>R Extracellular Domain Prevents GABA but not Pentobarbital Activation**

#### **6.1 Introduction**

##### *6.1.1 $\gamma$ -Aminobutyric Acid type A Receptors*

The  $\gamma$ -aminobutyric acid type A receptor (GABA<sub>A</sub>R) is a member of the Cys-loop family of ligand gated ion channels and mediates rapid inhibitory synaptic transmission in the mammalian nervous system. In addition to direct activation by the neurotransmitter GABA, the activity of GABA<sub>A</sub>Rs can be allosterically modulated by a variety of compounds including benzodiazepines (BZDs), barbitautes, volatile anesthetics, alcohols, and neuroactive steroids.<sup>1</sup> Identifying the mechanisms by which both GABA and these allosteric modulators affect the conformational movements within the GABA<sub>A</sub>R are critical for understanding the underlying actions of these pharmaceuticals.

The Cys-loop ligand gated ion channels (LGICs) are a superfamily with a common function and topology. In addition to the GABA<sub>A</sub>Rs, the superfamily contains two other inhibitory members, the GABA<sub>C</sub> and glycine (Gly) receptors, as well as two excitatory members, the nicotinic acetylcholine (nACh) and serotonin type 3 (5-HT<sub>3A</sub>) receptors. At rest these receptors are in a closed, non-conducting state. Binding of the appropriate neurotransmitter initiates a conformational change to an open, ion-conducting state. The conformational change from closed to open is called activation and the residues involved in the transition are part of the activation pathway.

Cys-loop LGICs are pentameric proteins with the five homologous subunits arranged pseudo-symmetrically around the central ion-conducting pore (Figure 6.1). In addition to numerous biochemical studies, structural information of these receptors has been aided by the crystal structure of the acetylcholine binding protein (AChBP)<sup>2</sup> and the cryo-EM structure of the *Torpedo californica* nicotinic acetylcholine receptor.<sup>3</sup> The primary sequence of each has a large amino-terminal extracellular domain followed by four membrane-spanning helices and a short extracellular carboxy-terminus. The extracellular domain consists primarily of two beta sheets with the beta strands connected by unstructured loops which contribute to the ligand binding site<sup>2,4</sup> and to the activation pathway.<sup>5-8</sup> The second transmembrane helix of each subunit lines the channel pore and contains the channel gate, some 50-60 Å from the neurotransmitter binding site.

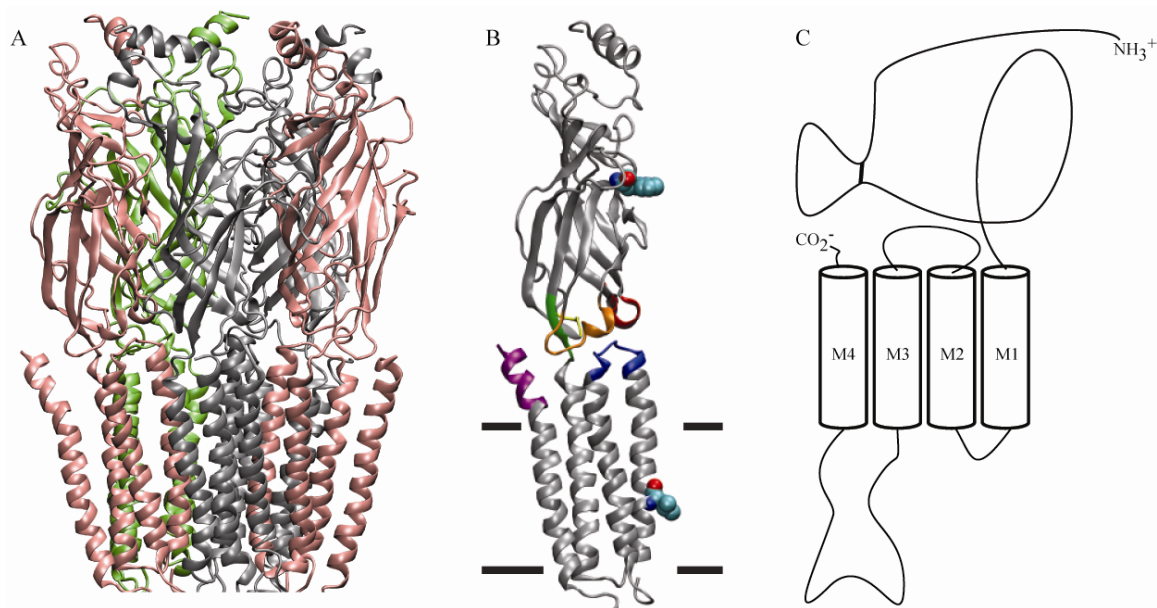


**Figure 6.1** General topology of GABA<sub>A</sub>R. **A**, homology model of the GABA<sub>A</sub>R (built from Protein Data Bank 2BG9) with the α subunits in pink, β subunits in gray, and the γ subunit in green. **B**, An individual subunit from **A** with the ligand binding site and channel gate highlighted as VDW and the edges of the membrane bilayer marked with black boxes. **C**, Schematic cartoon of each subunit. Each subunit has a predominantly beta sheet, N-terminal extracellular domain, four membrane-spanning helices, and a short extracellular carboxy terminus. The large intracellular loop between M3 and M4 has been omitted from **A** and **B**.

There are 19 identified GABA<sub>A</sub>R subunits designated  $\alpha_1$ - $\alpha_6$ ,  $\beta_1$ - $\beta_3$ ,  $\gamma_1$ - $\gamma_3$ ,  $\delta$ ,  $\epsilon$ ,  $\pi$ , and  $\theta$ , however not all combinations of subunits form functional receptors. In the mammalian brain, all GABA<sub>A</sub>Rs contain two  $\alpha$  and two  $\beta$  subunits.<sup>9</sup> The GABA binding site is located at the  $\beta/\alpha$  interface. The  $\beta$  subunit is considered the primary subunit of the binding site as it contributes four of the five residues in the aromatic box.<sup>10</sup> The  $\alpha$  subunit contributes the fifth residue to the binding site and is the complementary subunit. The fifth subunit of GABA<sub>A</sub>Rs is most commonly a  $\gamma_2$  subunit. Together  $\alpha_1\beta_2\gamma_2$ ,  $\alpha_2\beta_3\gamma_2$ , and  $\alpha_1\beta_2\gamma_2$  make up over two-thirds of GABA<sub>A</sub>Rs in the mammalian brain, with  $\alpha_1\beta_2\gamma_2$  comprising ~40% of all GABA<sub>A</sub>Rs.<sup>11</sup> Receptors containing  $\alpha_1$ - $\alpha_3$ , or  $\alpha_5$  and  $\gamma_2$  subunits are sensitive to clinically prescribed benzodiazepines (BZDs).<sup>12,13</sup> The BZD binding site is located at the  $\alpha/\gamma$  interface. Site-directed mutagenesis and substituted cysteine scanning methods (SCAM) have identified a histidine residue in loop A of the  $\alpha$  subunit (His101 in  $\alpha_1$  numbering) as critical to BZD action (Figure 6.2).<sup>14-16</sup>

Residues outside but near the aromatic box of Cys-loop receptors have been implicated in neurotransmitter binding and activation.<sup>17-23</sup> Mutagenesis and SCAM studies have identified residues  $\alpha_1$ N115,  $\alpha_1$ L117,  $\alpha_1$ R119,  $\alpha_1$ I120,  $\alpha_1$ T129, and  $\alpha_1$ R131 (Figure 6.2) that contribute to GABA binding.<sup>24,25</sup> The primary sequence of the  $\alpha_1$  subunit connects His101 to these residues through an unstructured (as indicated in the AChBP and cryo-EM structures) linker. Allosteric modulators of GABA<sub>A</sub>Rs bind at sites distinct from the GABA binding site and are believed to initiate an allosteric transition in the protein that indirectly modifies the conformation of the binding site.<sup>26</sup> Furthermore, numerous binding studies have shown that GABA and BZD binding is cooperative,<sup>25,27</sup>

providing additional evidence that the binding sites exert an effect on each other. Based on this evidence, we reasoned that the linker between His101 and N115 was critical to allosteric modulation and that cleavage of the backbone peptide in this region of the  $\alpha_1$  subunit would disrupt BZD potentiation of the GABA current. Herein, we use nonsense suppression<sup>28,29</sup> to site-specifically incorporate a photoactive unnatural amino acid to cleave the GABA<sub>A</sub>R backbone.

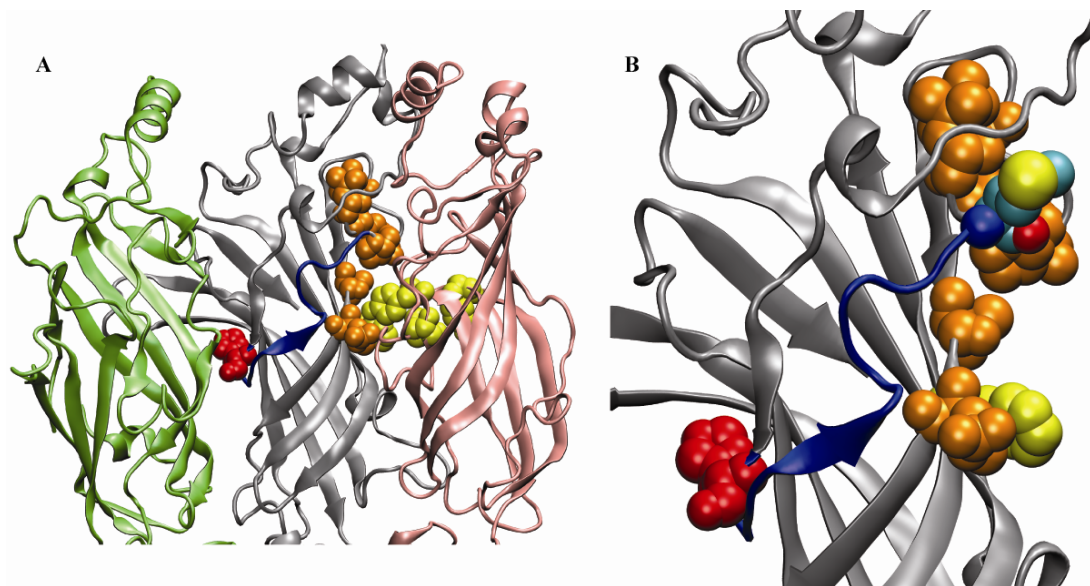
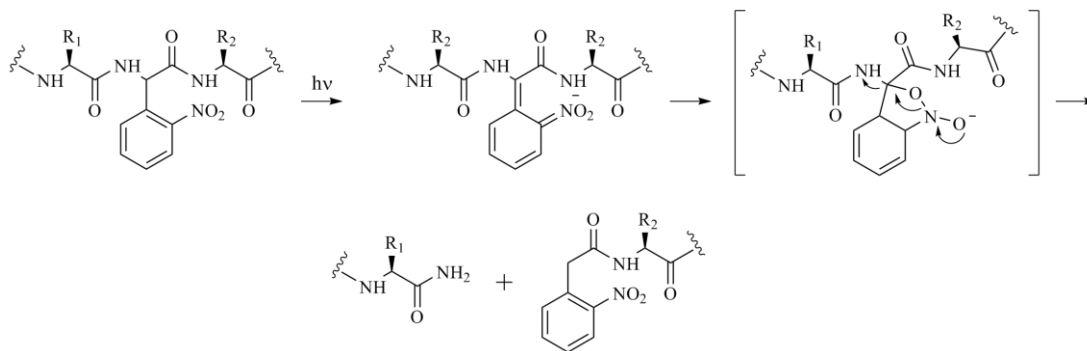


**Figure 6.2** An unstructured linker connects the GABA binding site and BZD binding site. **A**, the linker (blue) in the  $\alpha$  subunit (gray) stretches from the  $\beta/\alpha$  interface ( $\beta$  in pink) to the  $\alpha/\gamma$  interface ( $\gamma$  in green). His101 (loop A residue) is shown in red. Yellow residues denote the aromatic box for GABA. Orange residues have been shown to be involved in GABA binding but are not part of the aromatic box. **B**, Magnification of the linker region. M113 is added (cyan) to mark the site where Npg will be incorporated.

### 6.1.2 Proteolytic Cleavage by Photolysis

The design of nitrophenylglycine (Npg) was based on the photochemistry of 2-nitrobenzyl derivatives. Compounds of this type, including Npg, have been used as protecting groups in organic synthesis to produce caged neurotransmitters, ions, and second messengers that can be liberated photochemically.<sup>30-40</sup> When Npg is incorporated into a protein (Scheme 6.1), photolysis induces a series of rearrangements shown in Scheme 6.1, ultimately cleaving the peptide backbone.



Scheme 6.1

## 6.2 Results

### 6.2.1 Heterologous Expression of $GABA_A$ R

Expression of  $\alpha_1\beta_2\gamma_2$   $GABA_A$ Rs in heterologous expression systems such as *Xenopus* oocytes can result in a mixed population of  $\alpha_1\beta_2\gamma_2$  and  $\alpha_1\beta_2$  receptors.<sup>41</sup> When mRNA is injected in a 1:1:1 ratio, a mixed population results.  $\alpha_1\beta_2$   $GABA_A$ Rs are not modulated by BZDs, whereas  $\alpha_1\beta_2\gamma_2$   $GABA_A$ Rs are. Thus for a mixed population of receptors, we expect to see potentiation levels in between zero (expected for pure  $\alpha_1\beta_2$ ) and that of pure  $\alpha_1\beta_2\gamma_2$  populations ( $\sim 2.5$  for the benzodiazepine flurazepam). For wild type receptors, the relative amount of  $\gamma_2$  mRNA is increased until maximum potentiation is reached, and this ratio is used for additional experiments with conventional mutants.

When using the nonsense suppression methodology, expression depends on the batch of oocytes, relative expression levels of the mRNA, the quality of the tRNA-Uaa, and the oocyte's ability to incorporate the unnatural amino acid. Group observations<sup>1</sup> have indicated less consistency using the nonsense suppression methodology than seen with conventional mutagenesis. Specifically, we have found that expression levels vary considerably from one unnatural amino acid to another and from one batch of oocytes to

<sup>1</sup> Group observation from the labs of Dennis Dougherty, Division of Chemistry and Chemical Engineering, California Institute of Technology, Pasadena, CA 91125

the next. Therefore, we expected that an mRNA ratio for wild type recovery (incorporation of the wild type amino acid using the nonsense suppression methodology) would not necessarily work for our unnatural amino acids. Furthermore, the BZD potentiation test cannot be used since we expect our mutations to disrupt BZD potentiation. Due to these concerns, we decided to first conduct our experiments in the  $\alpha_1\beta_2$  GABA<sub>A</sub>R to determine if they should be carried over to the more complicated system of the  $\alpha_1\beta_2\gamma_2$  GABA<sub>A</sub>R.

Oocytes were injected with wild type  $\alpha_1$ ,  $\beta_{2S}$ , or  $\gamma_{2L}$  mRNAs individually. These oocytes did not respond to 10 mM GABA, indicating that the individual subunits were not sufficient to form functional GABA<sub>A</sub>Rs. As expected, oocytes injected with  $\alpha_1/\beta_{2S}$  mRNA gave functional GABA<sub>A</sub>Rs with an EC<sub>50</sub> of 1-3  $\mu$ M and a Hill coefficient between 1.2 and 1.8 for individual oocytes. Injection of  $\alpha_1/\gamma_{2L}$  or  $\beta_{2S}/\gamma_{2L}$  mRNA was not expected to produce receptors that respond to GABA. As anticipated,  $\alpha_1/\gamma_{2L}$  injected oocytes did not respond to GABA. However, the  $\beta_{2S}/\gamma_{2L}$  injected oocytes responded to GABA in a concentration-dependent manner. The EC<sub>50</sub> of the individual oocytes ranged from 70-200  $\mu$ M. All oocytes had Hill coefficients less than 1, providing a defining characteristic of this GABA<sub>A</sub>R subtype. GABA-induced responses in  $\beta_{2S}/\gamma_{2L}$  injected oocytes further complicate suppression experiments in the  $\alpha_1$  subunit of  $\alpha_1\beta_{2S}\gamma_{2L}$  GABA<sub>A</sub>Rs, providing another reason to first do experiments with  $\alpha_1\beta_{2S}$  GABA<sub>A</sub>Rs.

### *6.2.2 Site-Selection for Npg Incorporation*

The goal of structure-function studies is to elucidate the role of a particular residue in the wild type receptor. When using Npg and UV light we are effectively

making two mutations, the first is incorporation of Npg and the second is cleavage of the backbone. Differences in channel function before and after proteolysis provide information about the mutant Npg-containing receptor. However, we can still gain insight into the wild type receptor by selecting a site for Npg incorporation such that the mutant receptor has a similar pharmacology to the wild type receptor; thus candidate sites for Npg incorporation must be tolerant of side chain mutations.

While sites highly tolerant to side chain mutations are ideal for the analysis of Npg incorporation, these same sites can be problematic when using the nonsense suppression methodology. The complication arises from the orthogonality of the suppressor tRNA. In a nonsense suppression experiment, suppressor tRNA is charged with an unnatural amino acid (Uaa-tRNA). Once the unnatural amino acid is incorporated into the nascent protein, the uncharged suppressor tRNA (dCA-tRNA) is released back into the oocyte cytoplasm. If the suppressor tRNA is completely orthogonal, the amino-acyl transferases within the oocyte do not recognize dCA-tRNA as a tRNA molecule and thus will not charge the dCA-tRNA with a naturally occurring amino acid. However, if the dCA-tRNA is not completely orthogonal, it can be charged with an amino acid (re-aminoacylated) which can then compete for incorporation in place of the Uaa at the site containing the stop codon. Recent studies have shown that for THG73 (the suppressor tRNA used here), glutamine is most often the amino acid incorporated.<sup>42</sup>

One advantage to using electrophysiology to evaluate protein function is that our assays only detect functional receptors. Therefore, we use the control experiments explained below to identify candidate sites for Npg incorporation. For re-aminoacylation

control experiments, oocytes are injected with a mixture of uncharged dCA-tRNA and mRNA and tested for response to GABA. To control for read-through, oocytes are injected with only the mRNA and tested for response to GABA to ensure the ribosome does not read-through the stop codon. Finally, the wild type recovery control is conducted to ensure that suppression at the site of interest using the wild type residue reproduces wild type receptors. Ideally suppression sites with little or no response to GABA during the re-aminoacylation and read-through control experiments but high expression and wild type behavior during the recovery control will be identified.

**Table 6.1** Results of wild type recovery experiments at four sites in the  $\alpha\beta$  GABA<sub>A</sub>R

Site	Wild Type Recovery				Read-through	Re-aminoacylation
	EC <sub>50</sub> (μM)	n <sub>H</sub>	I <sub>max</sub> (μA)	N		
αβ (WT)	2.33 ± 0.04	1.4	-3.3 ± 0.7	9	N/A	N/A
αV107	3.4 ± 0.1	1.3	-4 ± 1	9	-0.08	-0.88
αM111	2.9 ± 0.2	1.3	-0.6 ± 0.4	10	-0.08	-0.03
αM113	2.3 ± 0.1	1.3	-2.3 ± 0.6	14	-0.06	-0.15
αP114	1.8 ± 0.1	1.7	-3.5 ± 0.5	5	-0.14	-0.08

I<sub>max</sub> values (μA) were determined from the same oocytes used to determine the EC<sub>50</sub> and Hill coefficients (n<sub>H</sub>). N is the number of oocytes used to determine the EC<sub>50</sub>, n<sub>H</sub>, and I<sub>max</sub>. Read-through and re-aminoacylation values are the average of the maximal current of two oocytes with the highest level of expression.

Npg is a beta-branched, hydrophobic amino acid, thus we reasoned it would be least likely to alter protein pharmacology at a site with hydrophobic and bulky side chains within the linker region. Therefore we selected V107, M111, M113, and P114 as candidate sites. Wild type recovery experiments at all four sites gave EC<sub>50</sub> values and Hill coefficients (n<sub>H</sub>) similar to the wild type  $\alpha\beta$  GABA<sub>A</sub>R. There was no appreciable difference in the shape of the dose response relationships (Figure 6.3, A). Oocytes injected with only the mRNA (read-through, Table 6.1) produced little current when tested with 10 mM GABA. When the mRNA was coinjected with dCA-tRNA, only the

$\alpha$ V107Tag $\beta$  showed significant current ( $I_{\max} > 300$  nA), such that the  $EC_{50}$  ( $6.5 \pm 0.3$   $\mu$ M) and Hill coefficient (1.0) could be determined.

**Table 6.2** Wild type recovery experiments at four sites in the  $\alpha\beta\gamma$  GABA<sub>A</sub>R

	$EC_{50}$ ( $\mu$ M)	$n_H$	$I_{\max}$ ( $\mu$ A)	N
$\alpha\beta\gamma$ (WT)	$55 \pm 2$	1.5	$-6 \pm 2$	7
$\alpha$ V107Tag $\beta\gamma$ + Val	$26 \pm 1$	1.6	$-10 \pm 1$	13
$\alpha$ M111Tag $\beta\gamma$ + Met	$49 \pm 2$	1.6	$-2.0 \pm 0.6$	11
$\alpha$ M113Tag $\beta\gamma$ + Met	$39 \pm 1$	1.5	$-6 \pm 1$	9
$\alpha$ P114Tag $\beta\gamma$ + Pro	$44 \pm 1$	1.5	$-6 \pm 1$	12

**Table 6.3** Results of read-through and re-aminoacylation experiments for nonsense suppression at four sites in the  $\alpha\beta\gamma$  GABA<sub>A</sub>R

Site	Read-through				Re-aminoacylation			
	$EC_{50}$ ( $\mu$ M)	$n_H$	$I_{\max}$ ( $\mu$ A)	N	$EC_{50}$ ( $\mu$ M)	$n_H$	$I_{\max}$ ( $\mu$ A)	N
V107	$330 \pm 70$	0.67	$-1.5 \pm 0.2$	8	$46 \pm 2$	1.19	$-5 \pm 1$	5
M111	$340 \pm 40$	0.72	$-1.0 \pm 0.2$	6	$1300 \pm 200$	0.73	$-3.4 \pm 0.9$	5
M113	$530 \pm 90$	0.64	$-1.3 \pm 0.1$	5	$1400 \pm 500$	0.60	$-3.7 \pm 0.8$	4
P114	$250 \pm 40$	0.73	$-1.2 \pm 0.3$	8	$38 \pm 3$	1.12	$-4.8 \pm 0.6$	3

Wild type recovery experiments in the  $\alpha\beta\gamma$  GABA<sub>A</sub>R gave  $EC_{50}$  and Hill coefficients similar to that of wild type at three of the four sites (Table 6.2, Figure 6.3, B). At V107, the  $EC_{50}$  was approximately half that of the wild type receptor.  $I_{\max}$  values were similar to wild type for M113 and P114, but significantly lower for M111. Read-through and re-aminoacylation controls gave whole cell currents large enough to determine the dose response relationships (Figure 6.3, C and D). All four sites had similar  $I_{\max}$ ,  $EC_{50}$ , and  $n_H$  values in the read-through experiments (Table 6.3). Re-aminoacylation of the tRNA and subsequent incorporation of the amino acid at V107 and P114 produced higher  $I_{\max}$  values than at M111 or M113 and  $EC_{50}$  values similar to wild type receptors.

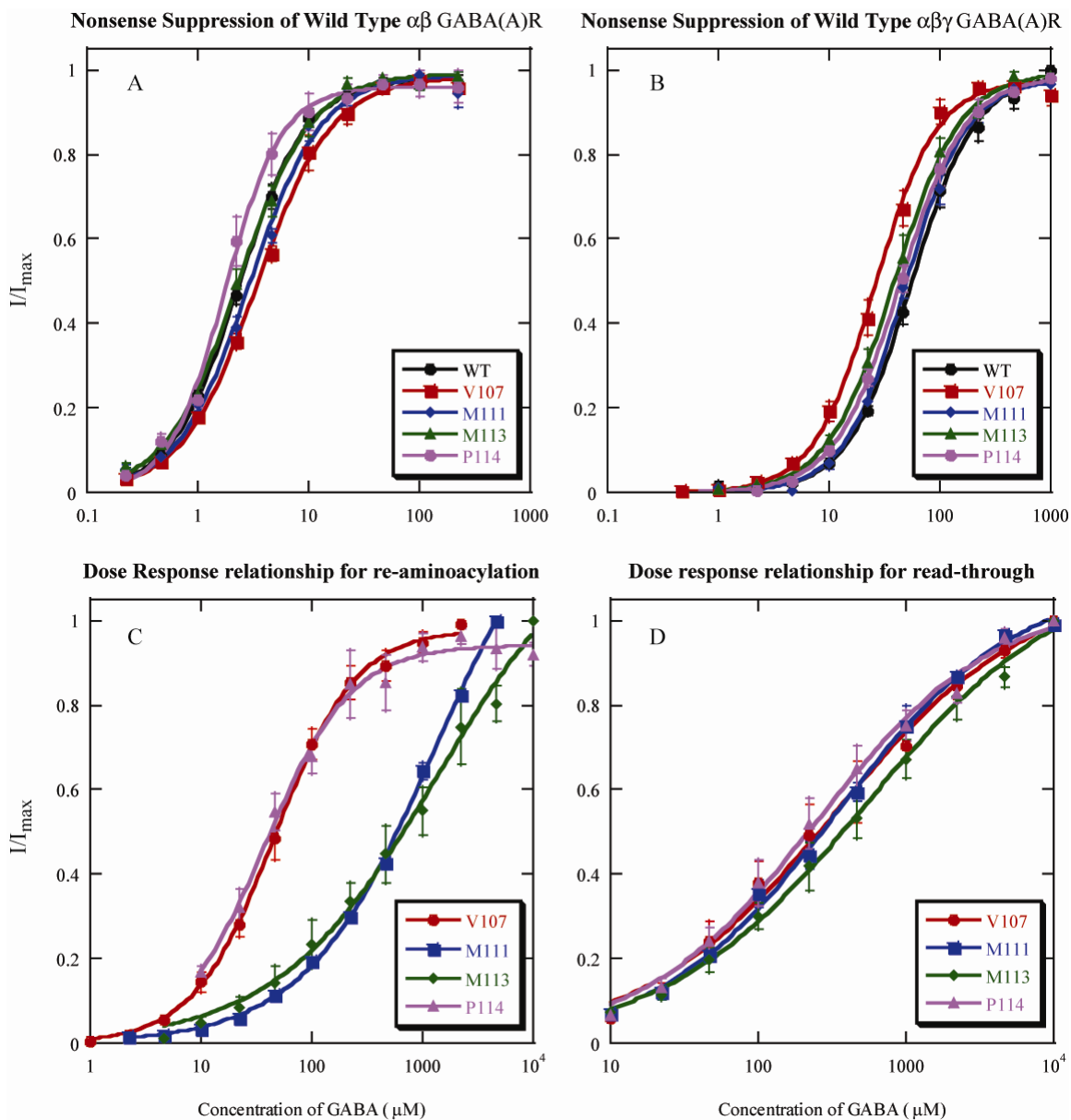


**Figure 6.3** Dose response relationships for control experiments using the nonsense suppression methodology at four sites (V107, M111, M113, and P114) in the  $\alpha$  subunit of the GABA<sub>A</sub>R. Wild type recovery in  $\alpha\beta$  GABA<sub>A</sub>R (A)  $\alpha\beta\gamma$  GABA<sub>A</sub>R (B). The GABA dose response relationship for re-aminoacylation of dCA-tRNA (C) and read-through (D)

Taken together, these results indicate that V107 and P114 would be poor sites for incorporation of Npg. V107 shows re-aminoacylation current in the  $\alpha\beta$  receptor. Furthermore, for both V107 and P114, re-aminoacylation and subsequent incorporation of the amino acid gave receptors with EC<sub>50</sub> values similar to wild type, suggesting it will be difficult to tell the difference between the pharmacology of the receptors containing

the unnatural amino acid and those resulting from re-aminoacylation. Both M111 and M113 gave receptors resulting from re-aminoacylation that are pharmacologically different from the wild type receptor. Of these two sites, M113 has higher  $I_{\max}$  values for wild type recovery in both the  $\alpha\beta$  and  $\alpha\beta\gamma$  receptors, suggesting M113 is the best site for Npg incorporation.

### 6.2.3 Incorporation of Npg at M113 of the $\alpha\beta$ GABA<sub>A</sub>R

The  $\alpha$ M113Npg $\beta$  mutant GABA<sub>A</sub>R functioned normally with a slight decrease in  $EC_{50}$  (Table 6.4). There was no significant difference in dose-response relationships, Hill coefficients, or macroscopic currents for wild type, wild type recovery ( $\alpha$ M113Met $\beta$ ), and mutant receptors (Figure 6.4).  $\alpha$ M113Npg $\beta$  receptors had lower  $I_{\max}$  values than wild type recovery, suggesting lower surface expression. We attribute the lower expression of the mutant receptor to using racemic Npg, as D-amino acids are unlikely to pass through the oocyte ribosome. Additionally, Npg is a  $\beta$ -branched amino acid, a structural type which is sometimes more difficult to incorporate using the nonsense suppression methodology.

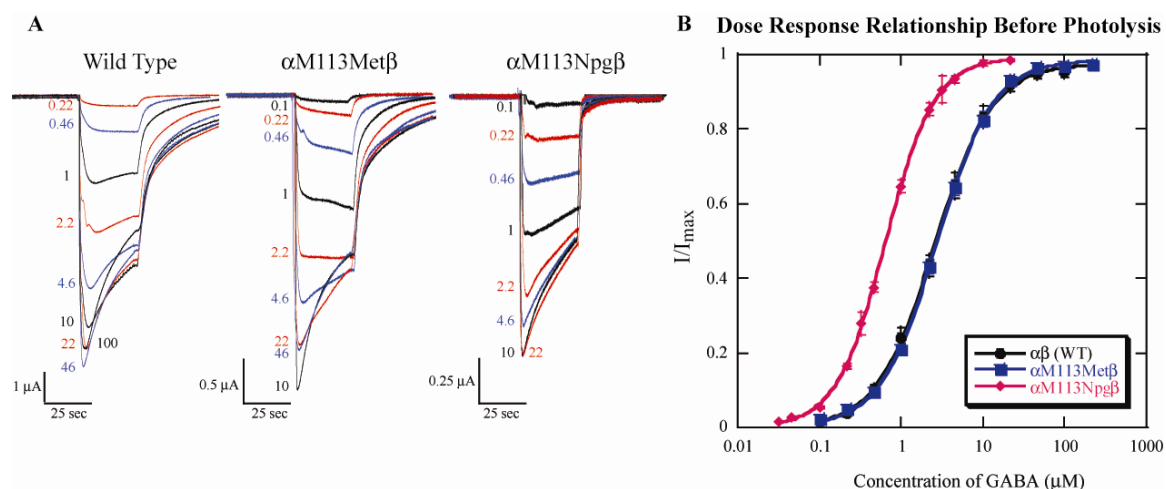


**Figure 6.4** Incorporation of Met and Npg at  $\alpha$ M113 gives similar macroscopic currents (A) and similarly shaped GABA dose response relationships (B) to the wild type receptor

**Table 6.4** EC<sub>50</sub> values for wild type recovery and Npg at  $\alpha$ M113

Receptor	EC <sub>50</sub> ( $\mu$ M)	n <sub>H</sub>	I <sub>max</sub>	N
$\alpha\beta$ (WT)	2.57 $\pm$ 0.05	1.25 $\pm$ 0.03	-4.2 $\pm$ 0.7	18
$\alpha$ M113Met $\beta$	2.72 $\pm$ 0.05	1.26 $\pm$ 0.03	-2.7 $\pm$ 0.4	32
$\alpha$ M113Npg $\beta$	0.57 $\pm$ 0.04	1.6 $\pm$ 0.2	-1.3 $\pm$ 0.1	25

#### 6.2.4 Proteolytic Cleavage of the $\alpha\beta$ GABA<sub>A</sub>R in Linker Region

The unnatural amino acid Npg was used to proteolytically cleave the fully folded GABA<sub>A</sub>R. The nitrophenyl group can absorb a photon of UV light and undergo a rearrangement that ultimately results in backbone cleavage of the peptide (Figure 6.1). Oocytes expressing  $\alpha$ M113Npg $\beta$  GABA<sub>A</sub>R were placed under a UV light source. Exposure time was monitored closely. Increasing the exposure of the  $\alpha$ M113Npg $\beta$  expressing oocytes led to a substantial decrease in the macroscopic current, an increase in EC<sub>50</sub>, and decrease in Hill coefficient (Table 6.5). After 8 hours of exposure to UV light whole cell currents of  $\alpha$ M113Npg $\beta$  expressing oocytes had decreased such that the EC<sub>50</sub> could be accurately determined. These whole cell currents are similar to those of the re-aminoacylation controls (Table 6.1). These data suggest photolysis is complete after 8 hours, and the remaining current is due to re-aminoacylation product.

To ensure these changes in current size, EC<sub>50</sub>, and Hill coefficients of  $\alpha$ M113Npg $\beta$  GABA<sub>A</sub>R expressing oocytes were due to cleavage of the backbone and not merely an artifact of exposure to light, control experiments with wild type GABA<sub>A</sub>R and  $\alpha$ M113Met $\beta$  GABA<sub>A</sub>R were conducted. Wild type GABA<sub>A</sub>R, expressed by injection of the wild type gene or by nonsense suppression, showed no trends in the magnitude of the whole-cell current, EC<sub>50</sub>, or Hill coefficient with increased exposure to UV light

(Table 6.5). These results suggest the decrease in macroscopic current is due to cleavage of the backbone by Npg rather than simply from exposing the oocytes to UV light.

**Table 6.5** Increased exposure to UV light decreases the whole cell current of oocytes expressing  $\alpha$ M113Npg $\beta$  but not wild type GABA<sub>A</sub>Rs.

Time	$\alpha$ M113Npg $\beta$				$\alpha$ M113Met $\beta$				$\alpha\beta$	
	EC <sub>50</sub>	n <sub>H</sub>	I <sub>max</sub>	N	EC <sub>50</sub>	n <sub>H</sub>	I <sub>max</sub>	N	I <sub>max</sub>	N
0 hours	0.57	1.6	-2.3 ± 0.3	8	4.2	1.3	-2.1 ± 0.7	7	-9.8 ± 2.2	4
2 hours	1.1	1.2	-0.6 ± 0.1	6	3.8	1.3	-2.6 ± 1.2	6	-6.6 ± 1.8	4
4 hours	1.1	1.2	-0.32 ± 0.07	8	2.6	1.5	-1.22 ± 0.09	6	-8.9 ± 0.9	4
6 hours	11	0.6	-0.20 ± 0.04	7	2.1	1.3	-1.3 ± 0.4	6	-8.4 ± 3.2	4
8 hours			-0.11 ± 0.05	7			-2.3 ± 0.9	4	-3.9 ± 0.9	4

*Note:* All these data were collected on the same day using oocytes from the same frog, injected at the same time. This extra measure was taken to control for differences in expression level due to any differences resulting from variability in batches of oocytes.

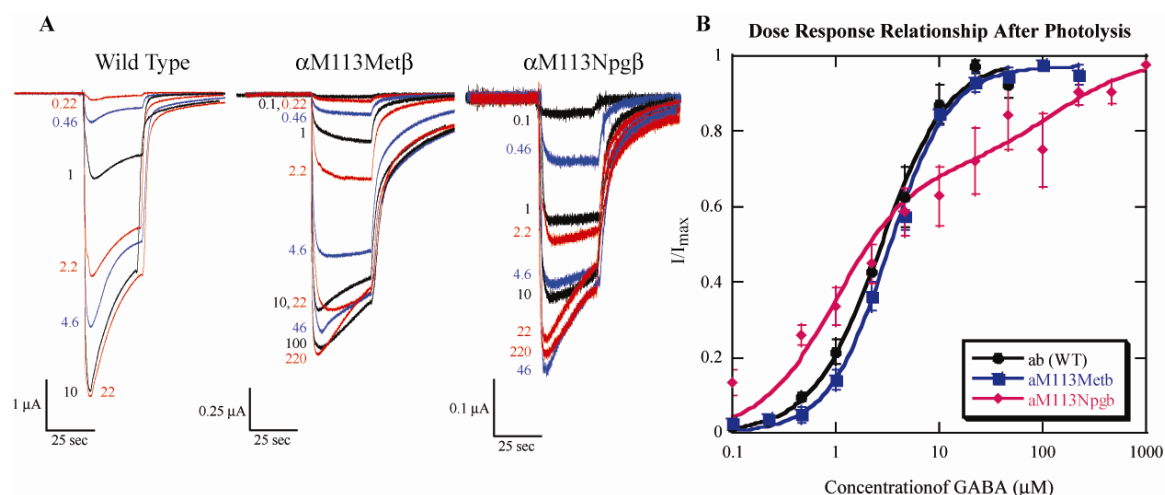


**Figure 6.5** 8 hours of exposure to UV light does not alter the macroscopic kinetics (A), or GABA dose response relationship (B) of wild type GABA<sub>A</sub>Rs. There is a decrease in the magnitude of the macroscopic currents of oocytes expressing  $\alpha$ M113Npg $\beta$  GABA<sub>A</sub>Rs after exposure to UV light, however, the overall shape of the trace remains the same (A). The GABA dose response relationship for GABA<sub>A</sub>Rs for wild type, wild type recovery, and  $\alpha$ M113Npg $\beta$  GABA<sub>A</sub>R after 8 hour exposure to UV light (B). Receptors cleaved at  $\alpha$ M113 are biphasic. For comparison to non-photolyzed oocytes, see Figure 6.4.

Once an eight hour exposure was determined to be sufficient for complete photolysis of Npg, these results were repeated on several batches of oocytes on different days to ensure these results were not due to anomalies occurring from the oocytes used (Table 6.6). On average, the EC<sub>50</sub> of the proteolyzed GABA<sub>A</sub>Rs increased 5.4-fold while the whole cell current decreased 89%. Despite the decrease in current size, the

macroscopic currents of the  $\alpha$ M113Npg $\beta$  GABA<sub>A</sub>R expressing oocytes exposed to UV light (Figure 6.5) have similar macroscopic kinetics to those that were not exposed to UV light (Figure 6.4) Wild type and  $\alpha$ M113Met $\beta$  GABA<sub>A</sub>Rs remained unchanged by exposure to UV light (Figure 6.5, Table 6.6).

**Table 6.6** Cumulative results of 8 hours of UV exposure

	Before UV exposure					After 8 hours UV exposure				
	EC <sub>50</sub>	n <sub>H</sub>	N	I <sub>max</sub>	N	EC <sub>50</sub>	n <sub>H</sub>	N	I <sub>max</sub>	N
WT	2.57 ± 0.05	1.3	18	9 ± 1	8	2.3 ± 0.3	1.6	5	5 ± 1	7
$\alpha$ M113Met	2.72 ± 0.05	1.3	32	1.9 ± 0.5	9	3.2 ± 0.2	1.5	7	2.5 ± 0.7	5
$\alpha$ M113Npg	0.57 ± 0.04	1.6	25	1.5 ± 0.2	23	3.1 ± 0.8	0.52	6	0.17 ± 0.03	24

*Note:* Higher expression of the wild type receptor caused greater scatter in the I<sub>max</sub> values. Although the I<sub>max</sub> value after exposure to UV light is ~55% of the before UV light value, we believe this difference is meaningless due to the high level of current seen in both cases.

### 6.2.5 Pentobarbital Activation of the $\alpha\beta$ GABA<sub>A</sub>R

Decreases in macroscopic current upon photolysis can be explained by having fewer surface expressed receptors, a decrease in the single-channel conductance, or a decrease in GABA activation. To determine which of these factors come into play, we studied GABA<sub>A</sub>R activation by the barbiturate pentobarbital. Pentobarbital (PB) binds to a completely different site from GABA, likely in the transmembrane region of the  $\beta$  subunits.<sup>43-45</sup> The single-channel conductance of PB activated GABA<sub>A</sub>Rs resembles those of GABA activated receptors, suggesting the open states of the ion channel are similar.<sup>46,47</sup> At low concentrations (<100  $\mu$ M), PB modulates GABA induced currents, while at higher concentrations PB directly activates GABA<sub>A</sub>Rs and at still higher concentrations blocks the receptors. Studies using the surface cysteine accessibility method with simultaneous fluorescence and electrophysiological recordings have established that PB activation of the GABA<sub>A</sub>R elicits conformational changes in the GABA<sub>A</sub>R that are different from those of GABA activation.<sup>48,49</sup>

If cleavage of the backbone by Npg leads to receptor endocytosis or a change in the single channel conductance, the maximal currents elicited by PB should decrease with photolysis. However, if proteolysis at  $\alpha$ M113 prevents activation of the receptor by GABA, we anticipate that PB currents should remain the same before and after photolysis. The dose response relationships of wild type and  $\alpha$ M113Npg $\beta$  GABA<sub>A</sub>Rs were determined both before and after photolysis (Figure 6.6). To reach saturation, concentrations of PB that block the receptor were used. In these cases the peak of the tail current was used as the measurement (Figure 6.6B).

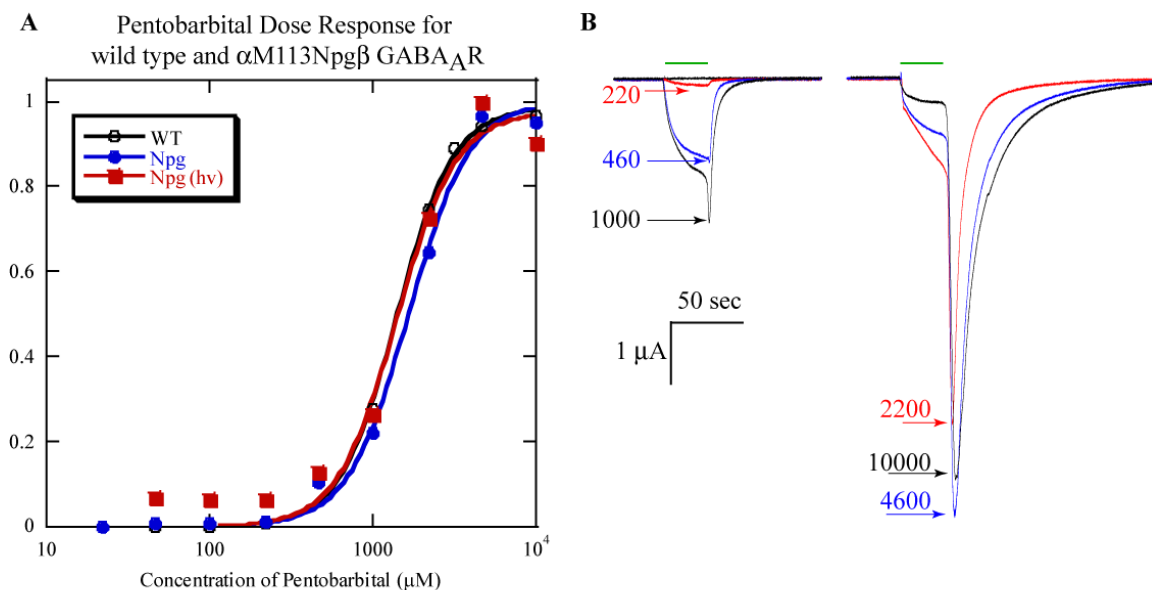


**Figure 6.6** Pentobarbital dose response relationships for wild type and  $\alpha$ M113Npg $\beta$  (before and after photolysis) GABA<sub>A</sub>R (A). PB induced currents of wild type GABA<sub>A</sub>R (B). Concentrations are in  $\mu$ M.

The PB dose response relationship for the  $\alpha$ M113Npg $\beta$  mutant before and after irradiation was not appreciably different from that of wild type (Figure 6.6). The EC<sub>50</sub> values were similar for wild type,  $\alpha$ M113Npg $\beta$ , and  $\alpha$ M113Npg $\beta$  after photolysis (1400, 1700, and 1400  $\mu$ M, respectively) as were the Hill coefficients (2.5, 2.3, and 2.4,

respectively). The dose response relationships indicate that in all three cases, 10 mM PB is sufficient to saturate the whole-cell current.

**Table 6.7** Macroscopic currents induced by exposure to Pentobarbital remain constant despite 8 hours of UV irradiation. Currents are reported in  $\mu\text{A}$ .

	Before UV exposure			After UV exposure		
	$I_{\text{GABA}}$	$I_{\text{PB}}$	N	$I_{\text{GABA}}$	$I_{\text{PB}}$	N
$\alpha\text{M113Met}\beta$	$4 \pm 2$	$4 \pm 1$	6	$3.7 \pm 0.4$	$4.1 \pm 0.5$	6
$\alpha\text{M113Npg}\beta$	$0.61 \pm 0.07$	$1.4 \pm 0.3$	12	$0.27 \pm 0.04$	$1.4 \pm 0.3$	12

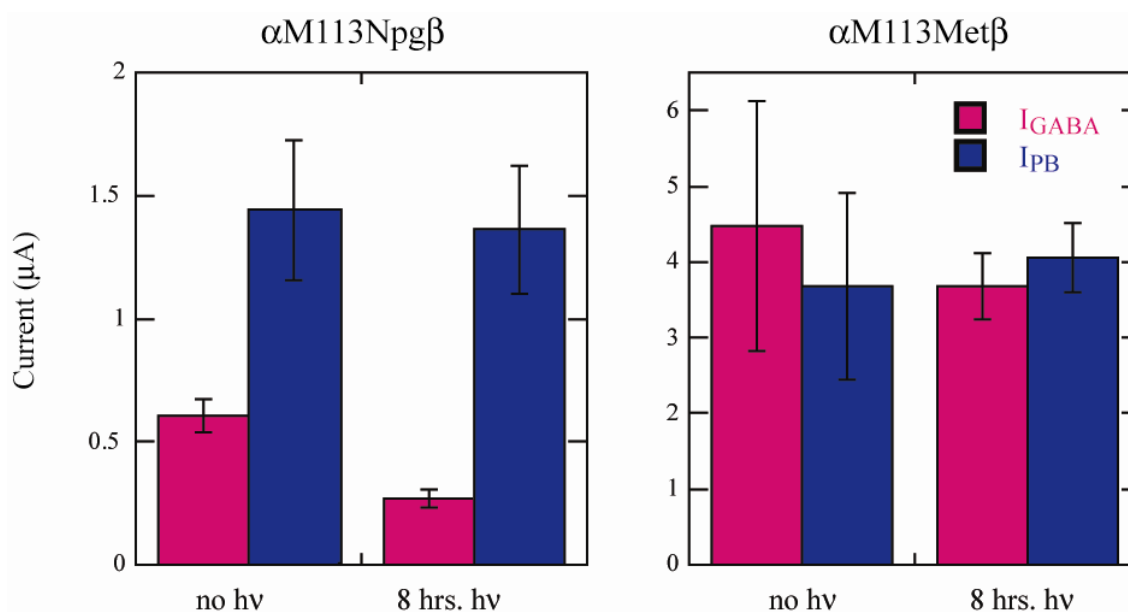


**Figure 6.7** Macroscopic whole-cell currents induced by saturating doses of GABA (pink) or pentobarbital (blue). *Left*: PB induced currents are unchanged by proteolytic cleavage of the  $\alpha\text{M113Npg}\beta$  mutant. *Right*: Control experiments with the wild type receptor

Macroscopic currents for wild type  $\text{GABA}_A\text{Rs}$  were similar in size for both agonists (Figure 6.7, Table 6.7) before and after UV exposure. These data indicate PB is a full agonist for the wild type receptor and, as expected, exposure of the wild type channel to UV irradiation does not alter channel function. The  $\alpha\text{M113Npg}\beta$  mutant shows larger macroscopic currents for pentobarbital than for GABA, indicating that the mutation lowers GABA but not PB efficacy. Proteolytic cleavage at  $\alpha\text{M113}$  had no

effect on PB induced currents (Figure 6.7, Table 6.7), suggesting the decrease in GABA induced currents is not due to endocytosis of the receptors or to a change in the single-channel conductance.

### 6.3 Discussion

The data indicate that proteolytic cleavage of the GABA<sub>A</sub>R backbone at  $\alpha$ M113 is sufficient to prevent GABA activation of the receptor. There are at least two possible causes of decreased activation. One possibility is that backbone cleavage alters the GABA binding site such that the receptor is unable to bind GABA. The second possibility is that proteolytic cleavage has disrupted the activation pathway for GABA. We have not explicitly investigated these two possibilities. However,  $\alpha$ M113 is well removed from the aromatic residues that form the GABA binding site.<sup>10</sup> Thus it seems unlikely that proteolytic cleavage at this site prevents GABA binding. Given the location of cleavage, the results from the pentobarbital studies, and work by others<sup>25,27</sup> implicating the linker region in the activation pathway of GABA<sub>A</sub>R, it seems unlikely that the backbone cleavage at  $\alpha$ M113 impedes binding of GABA to the receptor.

Given that disruption of GABA binding is unlikely, the reduction of macroscopic currents following proteolytic cleavage strongly suggests the linker connecting loops A and E of the complementary subunit of the GABA<sub>A</sub>R is a critical part of the activation pathway for GABA. Additionally, these data support the available structural information indicating that in the closed-state this region of the receptor is lacking a defined secondary structure.<sup>2,3</sup> If  $\alpha$ M113 was part of a  $\beta$ -sheet or  $\alpha$ -helix, the stabilizing backbone H-bond network might be expected to retain the overall structure following

proteolytic cleavage. Thus we would not expect the dramatic change in GABA activation seen here.

Although we hoped to study the role of the linker region in benzodiazepine modulation of GABA<sub>A</sub>Rs, we have restricted our studies to the BZD-insensitive  $\alpha_1\beta_2$  GABA<sub>A</sub>R. Extending these studies to the  $\alpha_1\beta_2\gamma_2$  GABA<sub>A</sub>R is unlikely to provide additional information about GABA or BZD activation pathways for the following reasons. The GABA binding sites of  $\alpha_1\beta_2$  and  $\alpha_1\beta_2\gamma_2$  GABA<sub>A</sub>Rs are essentially identical. Thus the conformational changes occurring in the  $\alpha$  subunit during GABA-induced activation are likely to be the same for both GABA<sub>A</sub>R subtypes. Therefore, we expect that proteolytic cleavage in the  $\alpha_1\beta_2\gamma_2$  GABA<sub>A</sub>R will be sufficient to prevent GABA activation of the receptor. BZDs modulate GABA-induced changes in the GABA<sub>A</sub>R, and without GABA activation we will not be able to detect the effects of BZD application. This reasoning, combined with the difficulty of nonsense suppression experiments in the  $\alpha$  subunit of the  $\alpha\beta\gamma$  receptor establish that incorporation of Npg and subsequent photo-induced cleavage of the linker backbone in the  $\alpha\beta\gamma$  GABA<sub>A</sub>R were not likely to provide additional insight into GABA<sub>A</sub>R function at present.

In conclusion, we find that proteolytic cleavage of the complementary  $\alpha_1$  subunit between loops E and A of the GABA<sub>A</sub>R is sufficient to prevent GABA activation, but not PB activation. These data indicate that the linker region is critical to normal receptor function and provide additional evidence that pentobarbital and GABA utilize different activation pathways within the same receptor.

## 6.4 Materials and Methods

### 6.4.1 Electrophysiology

*Mutagenesis and preparation of mRNA:* Human  $\alpha_1$ ,  $\beta_{2S}$ , and  $\gamma_{2L}$  GABA<sub>A</sub>R genes in pGEMHE were obtained from S.C.R. Lummis (Department of Biochemistry, University of Cambridge, Cambridge, United Kingdom). Quickchange PCR was used to make  $\alpha_1$ V107Tag,  $\alpha_1$ M111Tag,  $\alpha_1$ M113Tag, and  $\alpha_1$ P114Tag mutants and mutation was confirmed by sequencing (Laragen Sequencing). The cDNA was linearized using NheI (Roche) for the  $\alpha_1$  and  $\gamma_{2L}$  subunits and either SpeI (Roche) or SphI (Roche) for the  $\beta_{2S}$  subunit. The mMessage mMachine kit (Ambion) was used to generate capped mRNA for oocyte injection.

*Oocyte Injection:* Wild type  $\alpha_1\beta_{2S}$  mRNA was mixed in a 1:1 ratio and diluted to a final concentration of 100 ng/ $\mu$ l. Each oocyte was injected with 50 nL of mRNA mix, or 5 ng of mRNA mix.

For suppression experiments, a 5:1 mix of the mRNA of the mutated  $\alpha_1$  gene and  $\beta_{2S}$  at a final concentration of 1  $\mu$ g/ $\mu$ l was used. For wild type recovery experiments, this mRNA mix was mixed in a 1:1 (by volume) ratio with the deprotected aa-tRNA. Each oocyte was injected with a total volume of 50 nL of RNA mix; 25 ng mRNA and 15-50 ng of aa-tRNA. The aa-tRNA was stored with the amino group protected by an NVOC group. Prior to mixing the aa-tRNA with the mRNA mix, the aa-tRNA was deprotected by photolysis.

For Npg-tRNA, the amino group of Npg was protected by a 4-PO group. To deprotect Npg, a 1:1 mixture of Npg-tRNA and saturated aqueous iodide was made and allowed to sit at room temperature for 10 minutes. One equivalent of mRNA mix was

added and 50 nL of the mRNA/Npg-tRNA/ $I_{2(aq)}$  mixture was injected into each oocyte. This yielded a total of 16.7 ng each of mRNA and Npg-tRNA per oocyte.

Val- and Pro-tRNA were prepared as described previously.<sup>28,29,50</sup> Briefly, the amino acids were protected using a nitroveratryloxycarbonyl group and the carboxylic acid was activated as the cyanomethyl ester. The activated compound was coupled to the dinucleotide dCA, which was then enzymatically ligated to 74-mer THG73 tRNA<sub>CUA</sub> as detailed previously.

After injection, oocytes were incubated for 24-48 hours at 18°C prior to electrophysiology recordings. For a control, cRNA alone and cRNA mixed with dCA-THG (no unnatural amino acid attached) were injected into oocytes.

*Characterization of mutant receptors:* Peak GABA-induced currents were recorded at 22-25°C from individual oocytes using the OpusXpress system (Axon Instruments, Molecular Devices). A stock solution of 10 mM GABA (Sigma, St. Louis, MO) in ND96 buffer (in mM: 96 NaCl, 2 KCl, 1 MgCl<sub>2</sub>, 1.8 CaCl<sub>2</sub>, 5 HEPES, pH 7.5) was made fresh for each day's recording. Drug solutions were made from the stock by dilution in ND96 buffer. Drug was delivered to cells via the automated perfusion system of the OpusXpress. Glass microelectrodes were backfilled with 3 M KCl and had a resistance of 0.5-3.0 MΩ. The holding potential was -60 mV. To determine EC<sub>50</sub> values, GABA concentration-response data were fitted to the Hill equation (Equation 6.1), where  $I_{max}$  is the maximal peak current and n is the Hill coefficient.

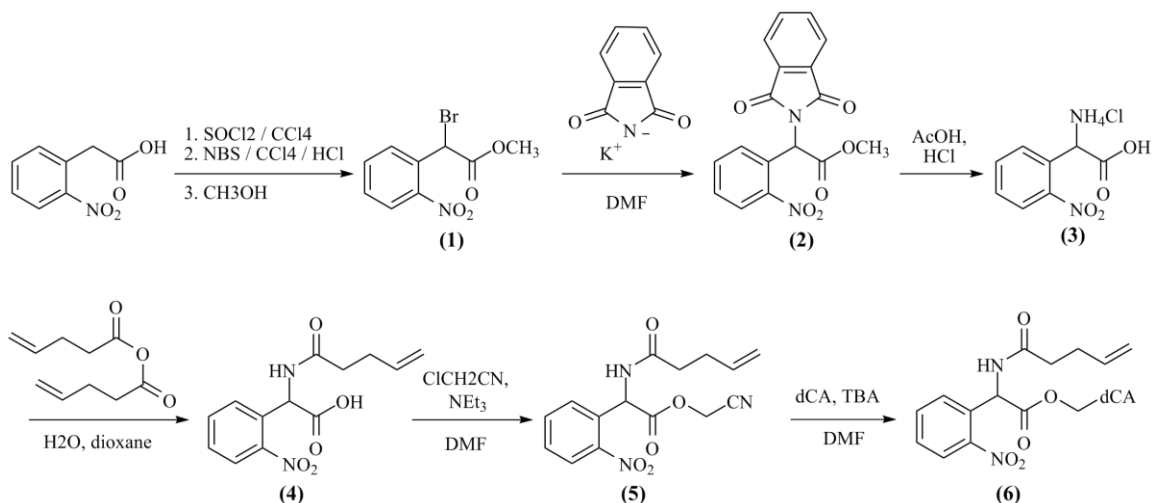
$$I = \frac{I_{max}}{1 + EC_{50} / [A]^n}$$

**Equation 6.1**

The dose-response relationship for pentobarbital (purchased as pentobarbital chloride from Aldrich) was determined in the same manner as GABA. For concentrations of pentobarbital that caused channel block, the tail current was used to determine  $I_{\max}$ . For determination of  $I_{\max}$  values from both GABA and PB, a high dose of GABA was applied, followed by a saturating dose of GABA ( $I_{\text{GABA}}$ ) and then a saturating dose of PB ( $I_{\text{PB}}$ ). PB solutions were stored at room temperature to minimize crystallization.

*Oocyte Irradiation:* Oocytes in ND96 containing theophylline and gentamicin as well as 4% horse serum were irradiated at 4°C in sterile 12 well polystyrene plates (Greiner bio-one Cellstar) with the lid in place. The irradiation source was a 288 W Hg lamp (BLAK-RAY Longwave Ultraviolet Lamp, Ultraviolet Products, San Gabriel, CA) equipped with a 360 nm band pass filter at a distance of 15-30 cm for a total of 8 hours, unless otherwise indicated. The proximity of the oocytes to the irradiation source caused significant warming of the bath solution, thus the oocyte bath solution (ND96<sup>+</sup> with 4% horse serum) was replaced every 1.5-2 hours to avoid excessive heating. Non-irradiated oocytes were maintained at 18°C. Prior to electrophysiology measurements, irradiated oocytes were placed in fresh ND96<sup>+</sup> with 4% horse serum at room temperature for at least 30 minutes. This improved the resting potentials and leak currents of the oocytes, but did not affect the dose response relationship or  $I_{\max}$  values.

## 6.4.2 Nitrophenyl Glycine Synthesis (Scheme 6.2)



Scheme 6.2

*Methyl- $\alpha$ -Bromo-*o*-nitrophenylacetate* (1) was prepared as described previously.<sup>50,51</sup> 2-Nitrophenyl acetic acid (3.0 g, 16.6 mmol), 10 mL of carbon tetrachloride were added to a 250 mL round bottom flask containing a stir bar. Addition of 10 mL (137 mmol) of thionyl chloride caused the reaction to turn orange/pink. A reflux condenser was attached and the reaction was heated to 55-60°C for 30 minutes. 3.61 g (20.3 mmol) of N-Bromosuccinimide in 25 mL of carbon tetrachloride and 10 drops of 6N HCl were added. The heat was adjusted to 65°C to bring the reaction to reflux. After 45 minutes black chunks were floating in the reaction mixture. After 3 hours, the reaction was cooled in an ice bath. While in the ice bath, 15 mL of MeOH was slowly added to the reaction mixture, followed by 50 mL of saturated aqueous sodium carbonate, turning the reaction mixture to a uniform brown-red liquid. The reaction mixture was extracted with 100 mL methylene chloride. The organic layer (red-brown, clear) was saved. The aqueous layer (brown, cloudy) was extracted with methylene

chloride until the organic layer was pale yellow and clear (5 x 70 mL). All methylene chloride layers were combined (clear, red liquid) and dried over magnesium sulfate. The magnesium sulfate was removed by filtration and the filtrate was run through a plug of alumina. The alumina was washed with another 300 mL of methylene chloride. The methylene chloride solution was concentrated and the various products were separated by silica gel column chromatography. The initial moving phase was 1:1 CH<sub>2</sub>Cl<sub>2</sub>:Hexane. The polarity of the moving phase was increased on a gradient to 5:3 CH<sub>2</sub>Cl<sub>2</sub>:Hexane then pure CH<sub>2</sub>Cl<sub>2</sub>. Pure EtOAc was used to remove all compounds from the column. Like fractions were combined and concentrated. Title compound was a pale, yellow solid. <sup>1</sup>H NMR (300 MHz, Figure 6.8) in CDCl<sub>3</sub>: δ7.92 (m, 2H), δ7.64 (m, 1H), δ7.46 (m, 1H), δ6.03 (s, 1H), and δ3.72 (s, 3H). Yield is 1.356 g (4.6 mmol, 28%).

*Methyl α-phthalimido-o-nitrophenyl acetate (2)*: 1.14 g (4.16 mmol) of **1** and 0.779 g (4.20 mmol) of potassium phthalimide (Aldrich) were placed in a 25 mL round bottom flask. 15.5 mL of DMF was added and the liquid immediately turned deep purple giving a cloudy, purple mixture. After 2 hours stirring at room temperature, the reaction was orange-yellow and cloudy. The precipitate (KBr) was removed by filtration giving a clear, orange/yellow filtrate. Addition of 20 mL chloroform and 50 mL water was used to separate the organic (cloudy, orange/yellow) and aqueous (cloudy, colorless) layers. After extraction of the aqueous layer (2 x 20 mL) with additional chloroform, the organic layers were combined, and dried over anhydrous sodium sulfate (Aldrich). Removal of the sodium sulfate by filtration yielded a clear, orange/yellow solution. After concentration and removal of DMF, a dark orange oil (1.444 g) remains. Hot ethanol was added, and a white powder precipitated out. The powder was isolated by filtration and

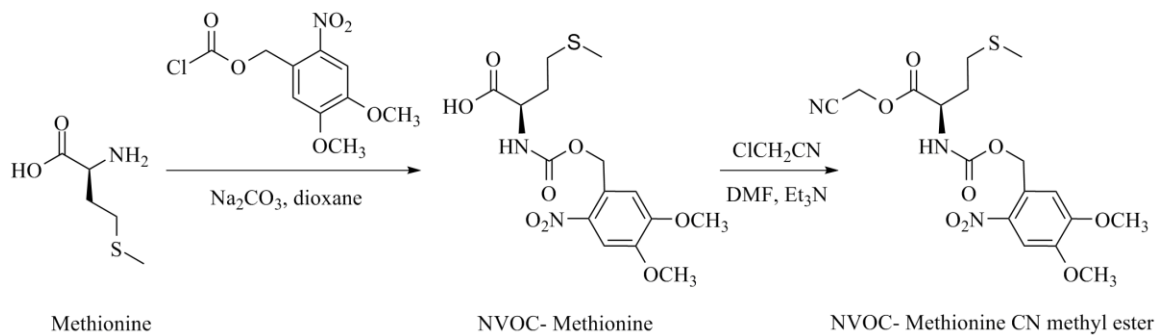
washed with water to give the title compound. Proton NMR (300 MHz, Figure 6.9) in  $\text{CDCl}_3$ :  $\delta$ 8.15 (d, 1H),  $\delta$ 7.9 (m, 2H),  $\delta$ 7.8 (m, 2H),  $\delta$ 7.55 (m, 2H),  $\delta$ 7.4 (d, 1H),  $\delta$ 6.95 (s, 1H),  $\delta$ 3.75 (s, 3H). Yield 0.89 g (2.62 mmol, 63%).

*o*-Nitrophenylglycine chloride salt (**3**): 2.6 mmol (0.89 g) of **2**, 6 mL of concentrated HCl and 4 mL of glacial acetic acid were combined in a 25 mL round bottom flask containing a stir bar. The reaction was slowly heated to 120°C and allowed to reflux. At reflux the solid dissolves giving a clear, yellow/orange solution. After 6.5 hours at reflux, the flask was cooled to room temperature overnight, then cooled to 5°C in an ice bath. Acidified (to pH=3.0 using HCl) water was added and the reaction was washed with ethyl acetate. The aqueous layer was concentrated yielding the title compound as a white solid. Proton NMR (300 MHz, Figure 6.10) in  $\text{D}_2\text{O}$ :  $\delta$ 8.15 (d, 1H),  $\delta$ 7.75 (t, 1H),  $\delta$ 7.6 (t, 1H),  $\delta$ 7.55 (d, 1H),  $\delta$ 5.37 (s, 1H). Yield: 0.363 g (1.56 mmol, 60%).

*4*-*PO*-Nitrophenylglycine (**4**): 1.56 mmol (0.363 g) of **3** was dissolved in 4 mL of water and 2.5 mL of dioxane. Sodium carbonate (0.498 g, 4.7 mmol) was added. Pent-4-enoic anhydride (0.314 g, 1.72 mmol) and 1.5 mL of dioxane were added. After stirring at room temperature for 3 hours, the reaction was poured into 25 mL of saturated  $\text{NaHSO}_4$  then washed with methylene chloride (3 x 25 mL). The aqueous layer was acidified with HCl to pH=2.5 (aqueous layer gets cloudy), then extracted with methylene chloride (3 x 25 mL). The methylene chloride layers were combined and concentrated to yield the title compound as a pale yellow solid.  $^1\text{H}$  NMR (300 MHz, Figure 6.11) in  $\text{CD}_3\text{OD}$ :  $\delta$ 8.06 (d, 1H),  $\delta$ 7.7 (m, 1H),  $\delta$ 7.62-7.53 (m, 2H),  $\delta$ 6.21 (s, 1H),  $\delta$ 5.8 (m, 1H),  $\delta$ 5.04-4.97 (m, 3H),  $\delta$ 2.42-2.28 (m, 4H). Yield is 0.142 g (0.52 mmol, 33%).

*Cyanomethyl ester of 4-PO-Nitrophenylglycine (5)*: 0.101 g (0.363 mmol) of **4** was added to a 5 mL round bottom flask containing a stir bar. After purging the flask with argon, 1 mL of chloroacetonitrile (15.8 mmol) and 150  $\mu$ l (1.07 mmol) of triethylamine were added. The reaction was stirred under argon overnight. Diethylether was used to dilute the reaction and then extracted against water. The organic layer was removed and dried over  $\text{MgSO}_4$ . The solvent was removed with reduced pressure leaving a yellow oil that still contained chloroacetonitrile. The excess chloroacetonitrile was removed by vacuum. The product was isolated by column chromatography (silica gel) starting with a solvent of 2:1 hexane:ethyl acetate, followed by 1:1, 1:2, and 1:4. A small yellow band still remained at the base of the column. MeOH was added to remove this band. Fractions were combined according to contents and the solvent was removed. The second isolated compound was the desired product (white powder). Proton NMR (300 MHz, Figure 6.12) in  $\text{CDCl}_3$ :  $\delta$ 8.18 (d, 1H),  $\delta$ 7.74-7.65 (m, 2H),  $\delta$ 7.58 (m, 1H),  $\delta$ 6.84 (d, 1H),  $\delta$ 6.17 (d, 1H),  $\delta$ 5.76 (m, 1H),  $\delta$ 5.0-4.97 (m, 2H),  $\delta$ 4.75 (d of d, 2H), 2.45-2.25 (m, 4H). Yield is 20 mg (0.063 mmol, 17.4%).

#### 6.4.3 Protection and Activation of Methionine (Scheme 6.3)



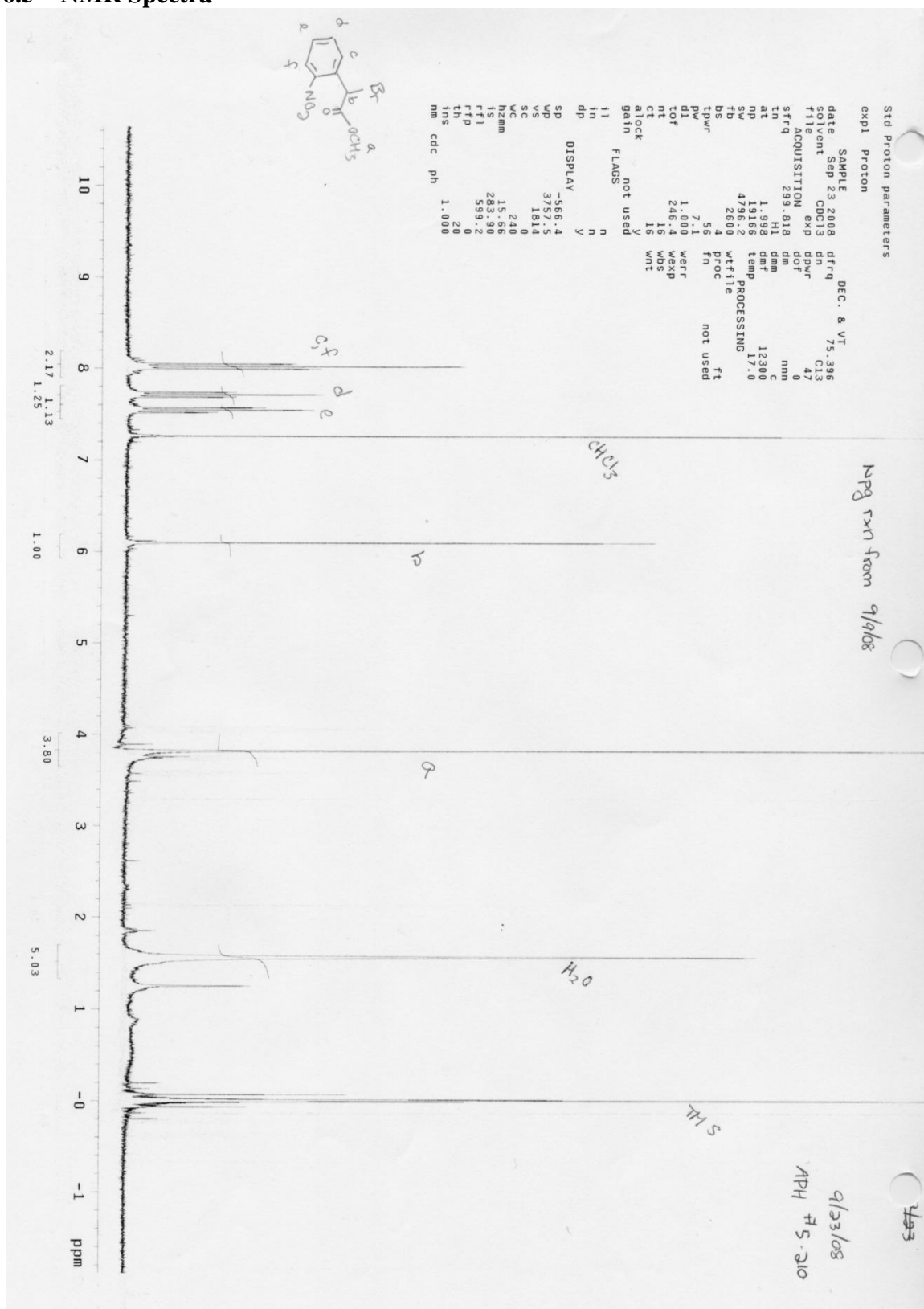
**Scheme 6.3**

*NVOC-Methionine*: In a 50 mL round bottom flask, sodium carbonate (0.832 g, 7.85 mmol) was dissolved in 8.25 mL of water to make a 10% weight/volume solution. While stirring, 0.300 g (2.01 mmol) L-methionine, then 5.75 mL of 1,4-dioxane were added. The flask was placed in an ice bath and 0.597 g (2.16 mmol) 4,5-dimethoxy-2-nitorbenzyl chloroformate (NVOC-Cl) was slowly added. Reaction became orange and cloudy. While stirring, the reaction was allowed to come to room temperature and turned yellow and cloudy. After 6 hours, the reaction contents were poured into 100 mL deionized water and washed with ether (3 x 45 mL). The organic layer was discarded. 6N HCl was added to the aqueous layer ( $\text{pH} \leq 2.0$ ) and a white precipitate crashed out of solution. The precipitate (pale yellow solid) was removed by filtration to give the title compound. Proton NMR (300 MHz, Figure 6.13) in  $\text{CDCl}_3$ :  $\delta 7.75$  (s, 1H),  $\delta 7.0$  (s, 1H),  $\delta 5.55$  (m, 2H),  $\delta 4.55$  (m, 1H),  $\delta 4.0$  (s, 3H),  $\delta 3.95$  (s, 3H),  $\delta 2.6$  (t, 2H),  $\delta 2.15$  (d of m, 2H), and  $\delta 2.1$  (s, 3H). Yield is 0.635 g (1.63 mmol, 81.3%).

*NVOC-Methionine cyanomethyl ester*: 0.384 g (0.989 mmol) NVOC-methionine was added to a 25 mL oven dried round bottom flask containing a stir bar. The flask was purged with argon and 3.2 mL dry DMF was slowly added. The solid dissolved to give a clear, yellow solution. 3.2 mL (50.6 mmol) chloroacetonitrile and 0.4 mL (2.87 mmol) triethylamine were added and the reaction was stirred under argon for 3 hours. The reaction as concentrated overnight by high vacuum leaving a yellow, sticky solid. Column chromatography (silica gel) was used to separate product from unreacted starting material. Initially the moving phase was 1:3 EtOAc: $\text{CH}_2\text{Cl}_2$  and was used to collect a yellow band. A yellow-orange band remained at the top of the column and was removed using 100% methanol. The first band contains the title compound. Fractions were

combined and concentrated to give a yellow solid. Proton NMR (300 MHz, Figure 6.14) in  $\text{CDCl}_3$ :  $\delta$ 7.72 (s, 1H),  $\delta$ 7.0 (s, 1H)  $\delta$ 5.62-5.47 (m, 2H),  $\delta$ 4.55 (m, 1H),  $\delta$ 4.01 (s, 3H),  $\delta$ 3.98 (s, 3H),  $\delta$ 2.61 (t, 2H),  $\delta$ 2.25-2.05 (d of m, 2H),  $\delta$ 2.11 (s, 3H). Yield is 0.188 g (0.435 mmol, 44%)

## 6.5 NMR Spectra

Figure 6.8 Proton NMR spectra of Methyl- $\alpha$ -Bromo-o-nitrophenylacetate (1)

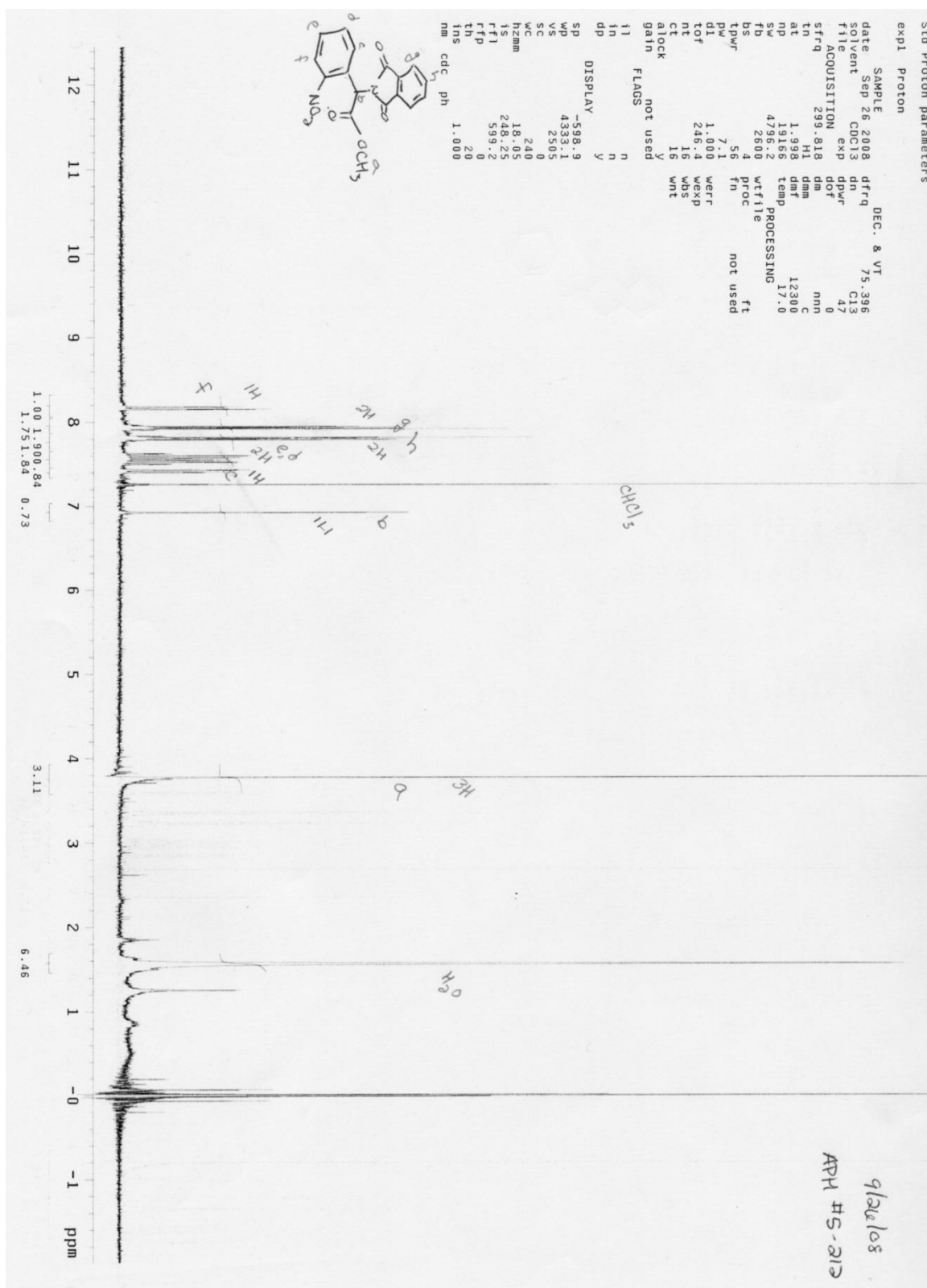


Figure 6.9 Proton NMR spectra of Methyl  $\alpha$ -phthalimido-o-nitrophenyl acetate (2)

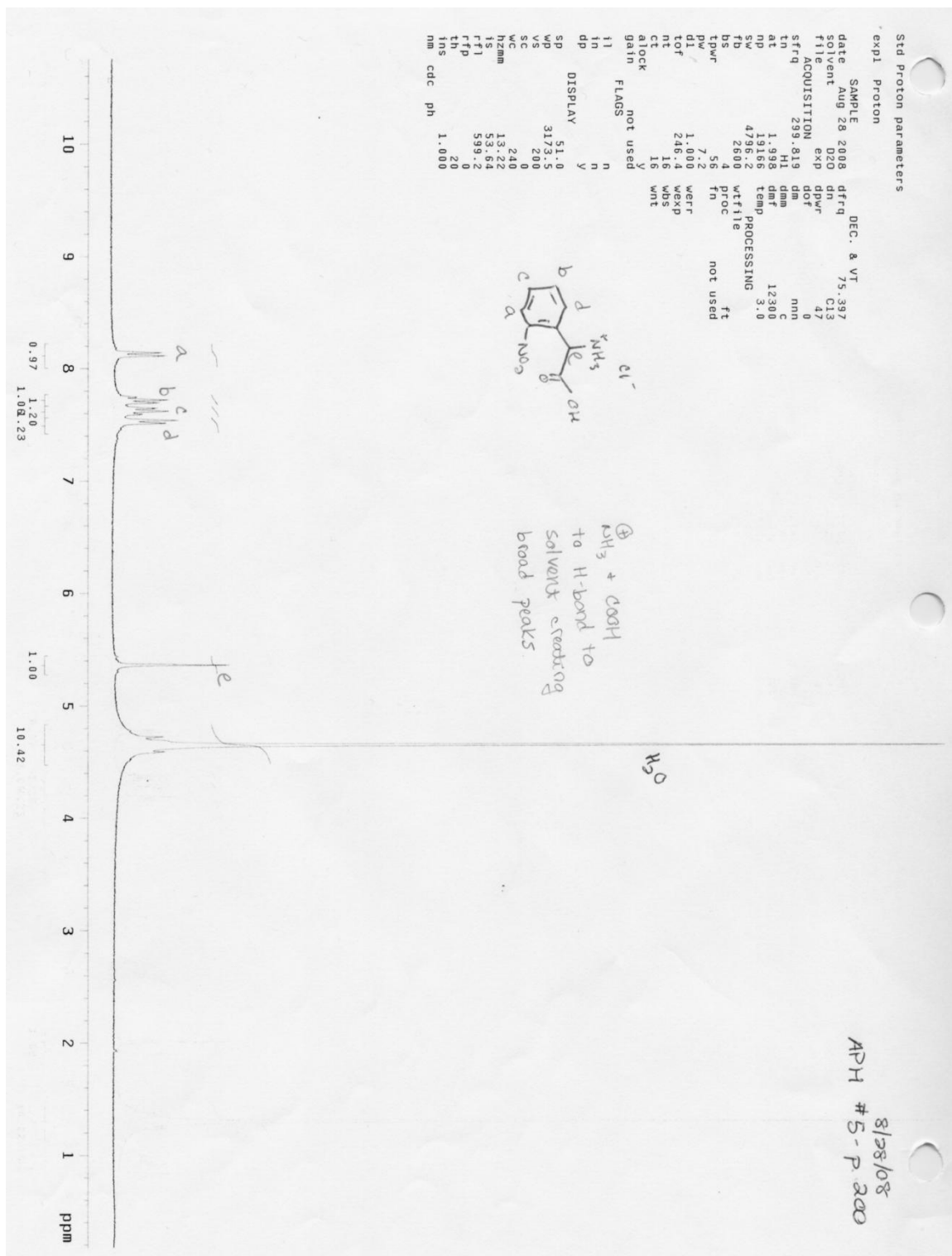


Figure 6.10 Proton NMR spectra of *o*-Nitrophenylglycine chloride salt (3)



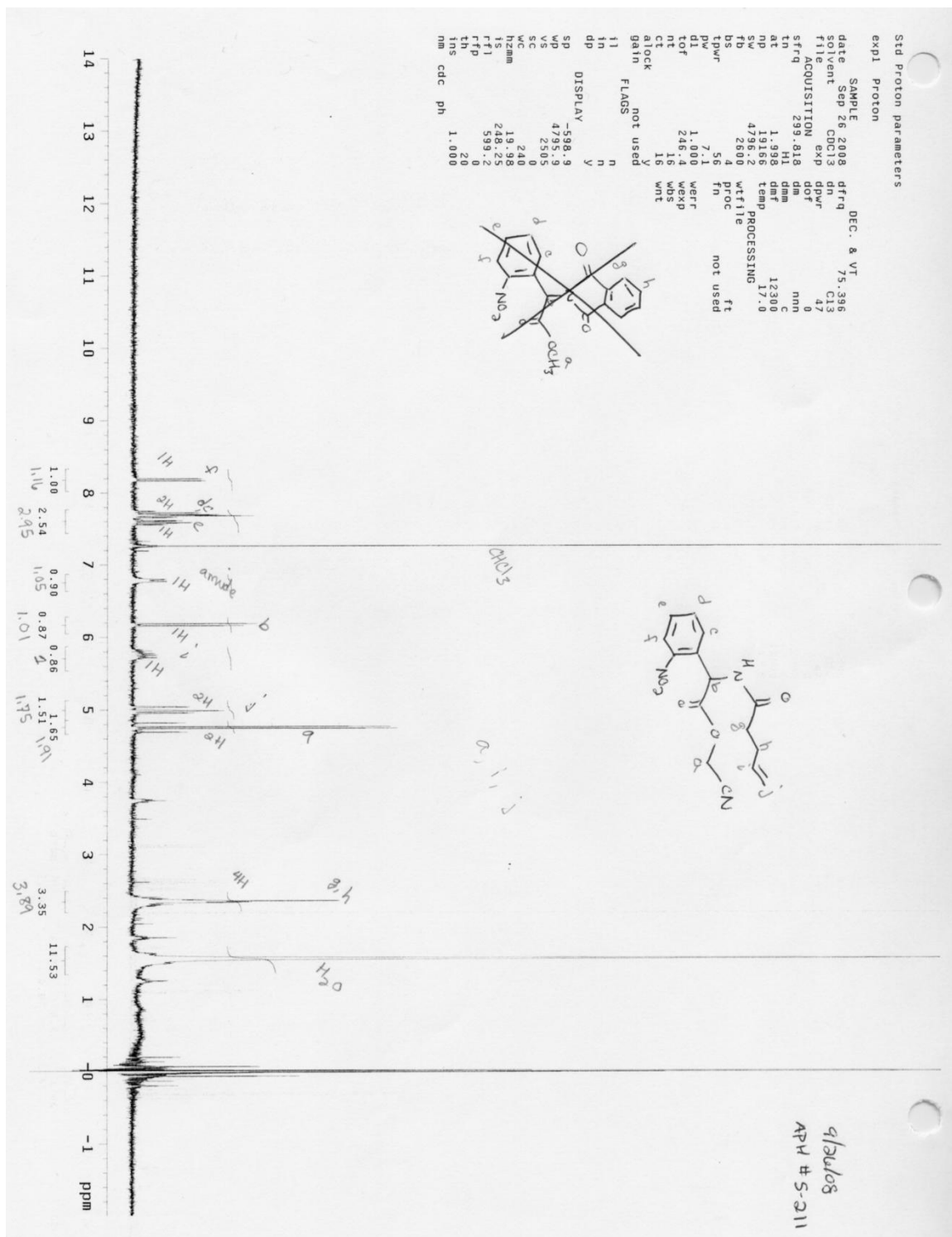


Figure 6.12 Proton NMR spectra of Cyano methyl ester of 4-PO-Nitrophenylglycine (5)



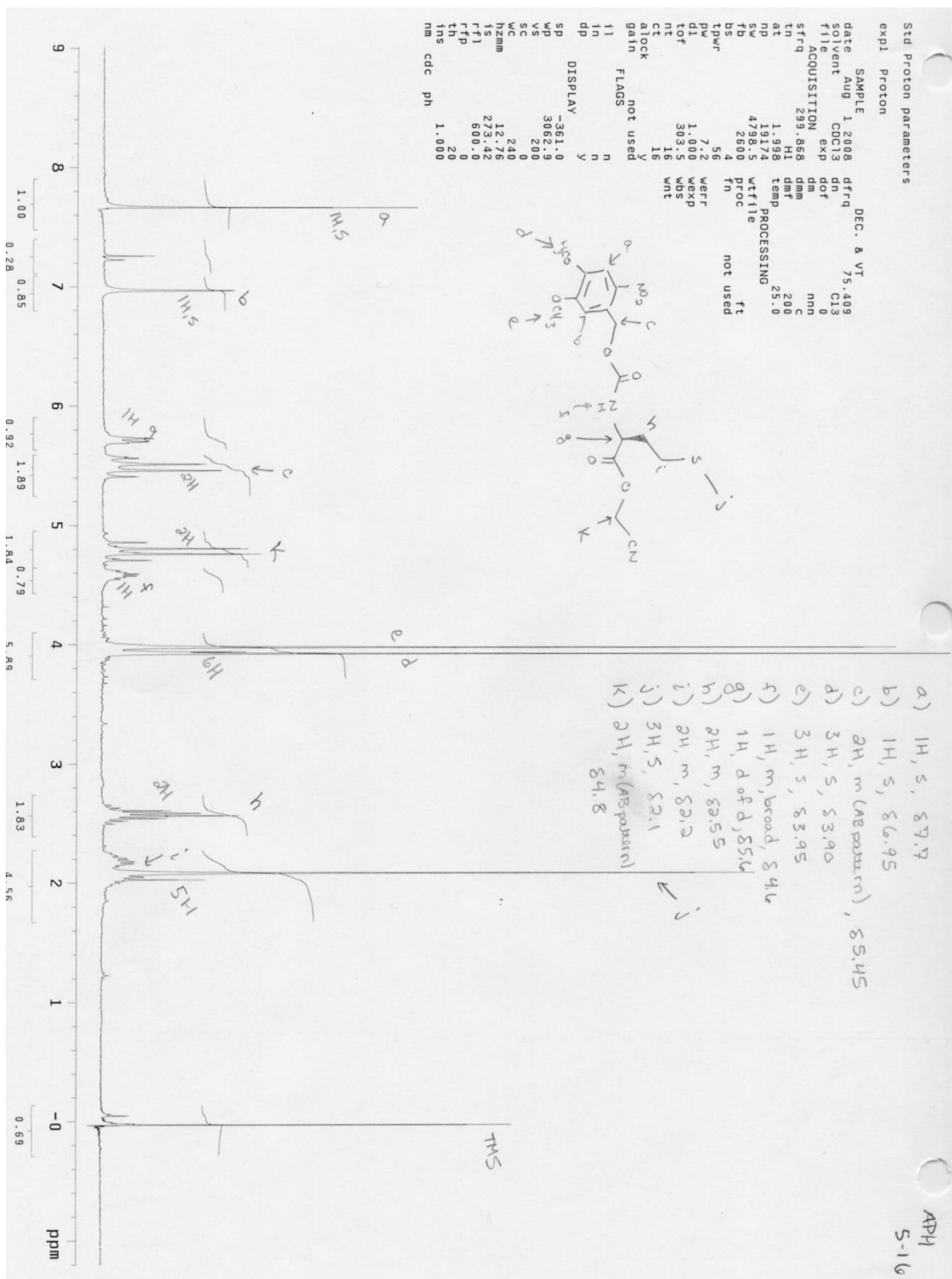


Figure 6.14 Proton NMR spectra of NVOC-Methionine CN methyl ester

## 6.6 References

- (1) Akabas, M. H. *Int Rev Neurobiol* **2004**, *62*, 1-43.
- (2) Brejc, K.; van Dijk, W. J.; Klaassen, R. V.; Schuurmans, M.; van Der Oost, J.; Smit, A. B.; Sixma, T. K. *Nature* **2001**, *411*, 269-76.
- (3) Unwin, N. *J Mol Biol* **2005**, *346*, 967-89.
- (4) Corringer, P. J.; Le Novere, N.; Changeux, J. P. *Annu Rev Pharmacol Toxicol* **2000**, *40*, 431-58.
- (5) Bouzat, C.; Gumilar, F.; Spitzmaul, G.; Wang, H. L.; Rayes, D.; Hansen, S. B.; Taylor, P.; Sine, S. M. *Nature* **2004**, *430*, 896-900.
- (6) Chakrapani, S.; Bailey, T. D.; Auerbach, A. *J Gen Physiol* **2004**, *123*, 341-56.
- (7) Hanek, A. P.; Lester, H. A.; Dougherty, D. A. *J Am Chem Soc* **2008**, *130*, 13216-8.
- (8) Xiu, X.; Hanek, A. P.; Wang, J.; Lester, H. A.; Dougherty, D. A. *J Biol Chem* **2005**, *280*, 41655-66.
- (9) Wafford, K. A. *Curr Opin Pharmacol* **2005**, *5*, 47-52.
- (10) Padgett, C. L.; Hanek, A. P.; Lester, H. A.; Dougherty, D. A.; Lummis, S. C. *J Neurosci* **2007**, *27*, 886-92.
- (11) Whiting, P. J. *Drug Discov Today* **2003**, *8*, 445-50.
- (12) McKernan, R. M.; Rosahl, T. W.; Reynolds, D. S.; Sur, C.; Wafford, K. A.; Atack, J. R.; Farrar, S.; Myers, J.; Cook, G.; Ferris, P.; Garrett, L.; Bristow, L.; Marshall, G.; Macaulay, A.; Brown, N.; Howell, O.; Moore, K. W.; Carling, R. W.; Street, L. J.; Castro, J. L.; Ragan, C. I.; Dawson, G. R.; Whiting, P. J. *Nat Neurosci* **2000**, *3*, 587-92.
- (13) Rudolph, U.; Crestani, F.; Benke, D.; Brunig, I.; Benson, J. A.; Fritschy, J. M.; Martin, J. R.; Bluethmann, H.; Mohler, H. *Nature* **1999**, *401*, 796-800.
- (14) Berezhnoy, D.; Nyfeler, Y.; Gonthier, A.; Schwob, H.; Goeldner, M.; Sigel, E. *J Biol Chem* **2004**, *279*, 3160-8.
- (15) Buhr, A.; Baur, R.; Malherbe, P.; Sigel, E. *Mol Pharmacol* **1996**, *49*, 1080-4.
- (16) Kucken, A. M.; Teissere, J. A.; Seffinga-Clark, J.; Wagner, D. A.; Czajkowski, C. *Mol Pharmacol* **2003**, *63*, 289-96.
- (17) Cashin, A. L.; Torrice, M. M.; McMenimen, K. A.; Lester, H. A.; Dougherty, D. A. *Biochemistry* **2007**, *46*, 630-9.
- (18) Gleitsman, K. R.; Kedrowski, S. M.; Lester, H. A.; Dougherty, D. A. *J Biol Chem* **2008**, *283*, 35638-43.
- (19) Lee, W. Y.; Sine, S. M. *J Gen Physiol* **2004**, *124*, 555-67.
- (20) Petersson, E. J.; Choi, A.; Dahan, D. S.; Lester, H. A.; Dougherty, D. A. *J Am Chem Soc* **2002**, *124*, 12662-3.
- (21) Price, K. L.; Bower, K. S.; Thompson, A. J.; Lester, H. A.; Dougherty, D. A.; Lummis, S. C. *Biochemistry* **2008**, *47*, 6370-7.
- (22) Wagner, D. A.; Czajkowski, C.; Jones, M. V. *J Neurosci* **2004**, *24*, 2733-41.
- (23) Xiu, X.; Puskar, N. L.; Shanata, J. A.; Lester, H. A.; Dougherty, D. A. *Nature* **2009**.
- (24) Cromer, B. A.; Morton, C. J.; Parker, M. W. *Trends Biochem Sci* **2002**, *27*, 280-7.
- (25) Kloda, J. H.; Czajkowski, C. *Mol Pharmacol* **2007**, *71*, 483-93.
- (26) Changeux, J. P.; Edelman, S. J. *Neuron* **1998**, *21*, 959-80.
- (27) Olsen, R. W. *Annu Rev Pharmacol Toxicol* **1982**, *22*, 245-77.
- (28) Nowak, M. W.; Gallivan, J. P.; Silverman, S. K.; Labarca, C. G.; Dougherty, D. A.; Lester, H. A. *Methods Enzymol* **1998**, *293*, 504-29.
- (29) Nowak, M. W.; Kearney, P. C.; Sampson, J. R.; Saks, M. E.; Labarca, C. G.; Silverman, S. K.; Zhong, W.; Thorson, J. S.; Abelson, J. N.; Davidson, N.; Schultz, P. G.; Dougherty, D. A.; Lester, H. A. *Science* **1995**, *268*, 439-442.
- (30) Adams, S. R.; Tsien, R. Y. *Annu Rev Physiol* **1993**, *55*, 755-84.
- (31) Gurney, A. M.; Lester, H. A. *Physiol Rev* **1987**, *67*, 583-617.
- (32) Kaplan, J. H.; Somlyo, A. P. *Trends Neurosci* **1989**, *12*, 54-9.
- (33) McCray, J. A.; Trentham, D. R. *Annu Rev Biophys Chem* **1989**, *18*, 239-70.
- (34) Mendel, D.; Ellman, J. A.; Schultz, P. G. *Journal of the American Chemical Society* **1991**, *113*, 2758-2760.

- (35) Milburn, T.; Matsubara, N.; Billington, A. P.; Udgaonkar, J. B.; Walker, J. W.; Carpenter, B. K.; Webb, W. W.; Marque, J.; Denk, W.; McCray, J. A.; et al. *Biochemistry* **1989**, *28*, 49-55.
- (36) Miller, J. C.; Silverman, S. K.; England, P. M.; Dougherty, D. A.; Lester, H. A. *Neuron* **1998**, *20*, 619-24.
- (37) Philipson, K. D.; Gallivan, J. P.; Brandt, G. S.; Dougherty, D. A.; Lester, H. A. *Am J Physiol Cell Physiol* **2001**, *281*, C195-206.
- (38) Ramesh, D.; Wieboldt, R.; Billington, A. P.; Carpenter, B. K.; Hess, G. P. *Journal of Organic Chemistry* **1993**, *58*, 4599-4605.
- (39) Wieboldt, R.; Gee, K. R.; Niu, L.; Ramesh, D.; Carpenter, B. K.; Hess, G. P. *Proc Natl Acad Sci U S A* **1994**, *91*, 8752-6.
- (40) Wieboldt, R.; Ramesh, D.; Carpenter, B. K.; Hess, G. P. *Biochemistry* **1994**, *33*, 1526-33.
- (41) Boileau, A. J.; Baur, R.; Sharkey, L. M.; Sigel, E.; Czajkowski, C. *Neuropharmacology* **2002**, *43*, 695-700.
- (42) Rodriguez, E. A.; Lester, H. A.; Dougherty, D. A. *RNA* **2007**, *13*, 1703-14.
- (43) Amin, J. *Mol Pharmacol* **1999**, *55*, 411-23.
- (44) Amin, J.; Weiss, D. S. *Nature* **1993**, *366*, 565-9.
- (45) Serafini, R.; Bracamontes, J.; Steinbach, J. H. *J Physiol* **2000**, *524 Pt 3*, 649-76.
- (46) Jackson, M. B.; Lecar, H.; Mathers, D. A.; Barker, J. L. *J Neurosci* **1982**, *2*, 889-94.
- (47) Rho, J. M.; Donevan, S. D.; Rogawski, M. A. *J Physiol* **1996**, *497 ( Pt 2)*, 509-22.
- (48) Mercado, J.; Czajkowski, C. *J Biol Chem* **2008**, *283*, 15250-7.
- (49) Muroi, Y.; Theusch, C. M.; Czajkowski, C.; Jackson, M. B. *Biophys J* **2009**, *96*, 499-509.
- (50) England, P. M.; Lester, H. A.; Davidson, N.; Dougherty, D. A. *Proc Natl Acad Sci U S A* **1997**, *94*, 11025-30.
- (51) Muralidharan, S.; Nerbonne, J. M. *Journal of Photochemistry and Photobiology B-Biology* **1995**, *27*, 123-137.